

# Experimental study of induced transparency or absorption and slow or fast light using orthogonally polarized whispering-gallery modes of a single microresonator

Khoa V. Bui and A. T. Rosenberger\*

Department of Physics, Oklahoma State University, Stillwater, OK, USA 74078-3072

## ABSTRACT

Induced transparency and absorption effects are observed in the throughput of a hollow bottle microresonator using either mode coupling or superposition of two co-resonant orthogonally polarized whispering gallery modes of very different quality factors ( $Q$ ). The first method is based on intracavity cross polarization coupling when either the TE mode or the TM mode is driven, resulting in coupled mode induced transparency (CMIT) and coupled mode induced absorption (CMIA). The second method is based on superposition of the throughputs when the two modes are simultaneously driven by input light linearly polarized at an angle of  $45^\circ$  with respect to the TE-TM basis of the resonator, and throughput of the same polarization is detected. In this way, superposition can be created even in the absence of cross polarization coupling. The observations using the second method are referred to as co-resonant polarization induced transparency and absorption (CPIT, CPIA). Co-resonance between the TE and TM modes can be obtained by strain tuning. The above behaviors are analogous to electromagnetically induced transparency and absorption (EIT, EIA), and enable slow light and fast light, i.e., the delay or advancement of an incident resonant pulse. Experimental results representative of several different types of behavior are presented here. Induced transparency is seen to be accompanied by pulse delay, whereas induced absorption can be accompanied by pulse advancement or delay. The results are analyzed and explained by simple analytical modeling and by comparison to the output of a more detailed numerical model describing these effects.

**Keywords:** slow light, fast light, hollow bottle microresonator, whispering-gallery modes

## 1. INTRODUCTION

The throughput of a single microresonator can exhibit induced transparency or induced absorption effects. In this work, these are observed when tunable laser light is injected via a tapered-fiber coupler into a fused-silica hollow bottle resonator (HBR)<sup>1</sup> that has two co-resonant (frequency-degenerate) whispering-gallery modes (WGMs) having very different quality factors ( $Q$ s). Induced transparency is generally accompanied by pulse delay (slow light), whereas induced absorption can show pulse delay or pulse advancement (fast light).<sup>2</sup> Two methods involving a pair of copropagating WGMs are investigated here. Co-resonance can be introduced in a controllable way by strain tuning (axial stretching of the HBR). The HBR has two orthogonally polarized families of modes, TE (transverse electric) and TM (transverse magnetic). Because the birefringence induced by strain tuning causes the two types of modes to tune at different rates, it can be used to impose frequency degeneracy between a TE mode and a TM mode.<sup>3-5</sup>

The first method for achieving induced transparency and absorption uses cross-polarization coupling (CPC). Light of one polarization circulating in a WGM of the microresonator can be coupled into a co-resonant WGM of the orthogonal polarization. This CPC is likely a result of weak polarization rotation, but for our purposes it can be thought of as weak scattering. In this case, the input light and detected throughput are of one polarization, say TE. Because of CPC, the interaction with a co-resonant TM WGM produces a throughput spectrum (as the driving laser is scanned in frequency) showing cross-polarization coupled-mode induced transparency and absorption (CMIT, CMIA).<sup>6,7</sup> An input pulse whose center frequency is resonant will be delayed or advanced. These effects are similar to the coupled-resonator-induced transparency and absorption (CRIT, CRIA) observed in coupled whispering-gallery microresonators,<sup>8,9</sup> except that output from the non-driven WGM can also be detected here.

\*atr@okstate.edu; phone 1 405 744-6742; fax 1 405 744-6811; physics.okstate.edu/rosenber/index.html

In the case of CMIT and CMIA, the light incident on the microresonator is linearly polarized so as to directly excite only one family of modes, say TE, and the mode coupling effects are observed as a splitting or modification of the shape of the resonant TE throughput dip. The second method uses incident light linearly polarized at 45° (in this work) in the TE-TM basis to drive coresonant modes of the two polarizations and produce induced transparency or absorption in the throughput of the same linear polarization as the incident light. This occurs even in the absence of cross-polarization mode coupling, demonstrating that mode superposition is sufficient to produce these effects, including pulse delay or advancement. The effects induced in this manner are referred to as coresonant polarization induced transparency and absorption (CPIT, CPIA).<sup>6,7</sup>

A simple ring-cavity model has been used to study the effects observed in the two methods. Numerical application of the model can be used to produce plots that can be used for comparison with experimental results. In this fitting procedure, there are two adjustable parameters: the CPC strength is a nearly free parameter, having only weak constraints set by other experimental observations; the offset of the two WGMs from coresonance is a semi-free parameter, being rather tightly constrained by observation of the throughput dips of the two WGMs. The model also gives analytical results that can be used in evaluation of the experimental-numerical fit.<sup>10</sup> Several examples of the two methods will be presented here, with experimental results compared to numerical and analytical results.

## 2. MODEL

The model is described in more detail in our other contribution to this volume.<sup>10</sup> Experimentally measured quantities used as input data for the numerical program include: the HBR radius  $a$ , the effective refractive index of the mode  $n$ , and the optical wavelength  $\lambda$ ; the polarization angle of the input and throughput light; the input/output coupling regimes of the two WGMs; the throughput dip depths and  $Q$  values of the two WGMs, measured independently (when significantly offset from coresonance); and the temporal width of an input Gaussian pulse (bandwidth < IT/IA window width). Having  $a$ ,  $n$ , and  $\lambda$ , then  $Q_j$  ( $j = 1,2$ ) gives us the total loss,  $T_j + \alpha_j L$ , coupling loss plus intrinsic loss. Knowing the coupling regime (determined by artificially increasing the effective intrinsic loss momentarily by touching the other side of the HBR with another fiber) tells us whether the loss ratio,  $x_j = T_j / \alpha_j L$ , is  $> 1$  (overcoupled) or  $< 1$  (undercoupled), and this allows determination of  $x_j$  and thus the individual losses using the throughput dip depth, which is given by

$$M_j = \frac{4x_j}{(1+x_j)^2}. \quad (1)$$

Thus all the parameters needed for the model are experimentally measured except the two that are (semi-) free for fitting.

## 3. EXPERIMENT

A typical HBR, fabricated from fused-silica capillary tubing, is shown in Fig. 1. The capillary is internally etched with a hydrofluoric acid solution to thin its walls to a thickness of 5-10  $\mu\text{m}$ , and then a short length is heated using a hydrogen torch while under internal air pressure, leading to the formation of a bottle-shaped bulge.<sup>1</sup> In the HBRs actually used in the experiments, the bulge diameter is around 340  $\mu\text{m}$ . A WGM in an HBR is specified by three indices in addition to its polarization: an integral number of wavelengths around the circumference is specified by the azimuthal mode index, the radial index gives the number of radial intensity maxima, and the axial index gives the number of axial field nodes. Because WGMs of higher radial order are confined by the internal surface as well as the external surface, the HBR is well suited to sensing of an internal analyte. For our purposes, since we want one WGM with a high  $Q$  and one with a low  $Q$ , the extra surface scattering of a high-radial-order WGM makes low  $Q$  easier to find. Also, strain tuning by axial stretching is easy to implement.

The input/output coupling is done by bringing a tapered single-mode fiber tangent to the HBR, perpendicular to its axis. A typical setup is sketched in Fig. 2. The microresonator and tapered coupling fiber are enclosed in a transparent plastic box (not shown) to help keep them clean and isolated from air currents. Also not shown are the translation stages that are used for precise positioning of the tapered fiber with respect to the microresonator, and the piezo-controlled strain tuner that allows tuning of WGM frequencies.

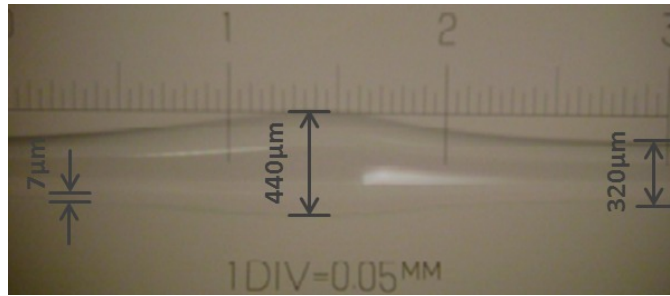


Figure 1. Hollow bottle resonator (HBR) made from 320- $\mu\text{m}$  OD fused-silica capillary, HF-etched to a wall thickness of 5-10  $\mu\text{m}$ , and expanded to a maximum bulge diameter of 440  $\mu\text{m}$ . The axial length of the resonator is approximately 1.5 mm.

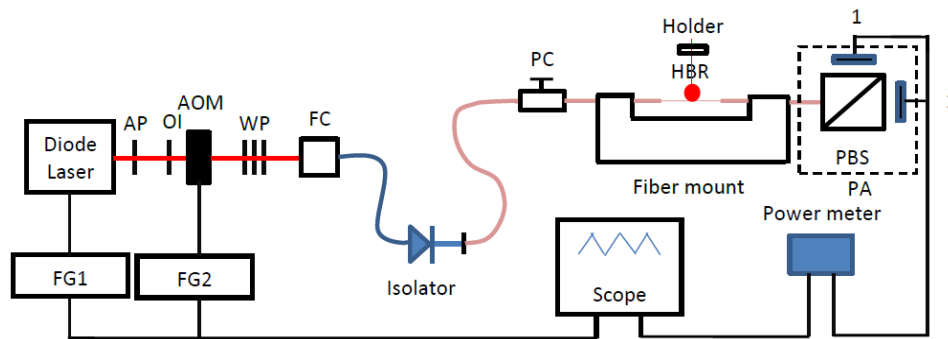


Figure 2. Experimental setup. A detailed description is given in the following paragraph.

A tunable diode laser (1508-1662 nm) is frequency scanned by function generator FG1. Its free-space output beam passes through an anamorphic prism (AP) and optical isolator (OI), and is amplitude-modulated (if Gaussian-pulse input is desired) by an acousto-optic modulator (AOM) controlled by arbitrary waveform generator FG2. The beam passes through a set of waveplates (WP) for polarization control before a fiber coupler (FC) launches it into a fiber isolator for reduction of Fabry-Perot fringes that might result from multiple reflections in the fiber. A final polarization controller (PC) permits adjustments to the polarization before the light enters the tapered fiber adjacent to the microresonator. This region of fiber is kept short and straight to preserve the polarization; the light exiting it is collimated and split by a polarizing beam splitter (PBS). Detectors 1 and 2 then measure the powers in the orthogonal polarization components of the throughput light. The entire polarization analyzing system (PA) can be rotated about the fiber axis, permitting arbitrary rotation of the detection polarization basis with respect to the microresonator's polarization basis. The input light is linearly polarized, either parallel to an HBR eigenpolarization for CMIT/CMIA experiments, or at  $45^\circ$  for CPIT/CPIA experiments. For pulse response experiments, one detector is chosen to have a fast response.

#### 4. RESULTS

Some typical results are presented in this section. In each figure, experimental and numerical results are presented in separate plots. The experimental throughput is the normalized detector response, where the horizontal axis of the oscilloscope trace has been converted to frequency based on the laser scan range and speed. The experimental pulse traces have been fitted by Gaussians for comparison to the numerical output. For some of the analytical comparisons, it is helpful to have an expression for the coupling loss  $T_j$ , which can be found from the measured values of  $Q_j$  and  $M_j$  by inserting  $Q_j$  and  $x_j$  (found from  $M_j$ ) into the following expression:

$$T_j = \frac{4\pi^2 na}{\lambda Q_j (1 + x_j^{-1})}. \quad (2)$$

For each example, the values of the measured quality factors and dip depths are given, along with the coupling regimes; then the fitted values of the CPC strength  $T_s$  and the frequency offset of the higher- $Q$  WGM from the lower- $Q$  WQM are specified.

The numerical fits are not perfect, and in most cases this can probably be attributed to the presence of other WGMs in the experiment. WGMs that overlap with the WQMs of interest can affect the measurements of dip widths and depths, and nearby WGMs can result in an effective amplitude shift of the off-resonance throughput.

#### 4.1 CMIT/CMIA

Three examples are presented here. Figure 3 is a case of CMIT, Fig. 4 is CMIA with pulse advancement, and Fig. 5 is CMIA with pulse delay.

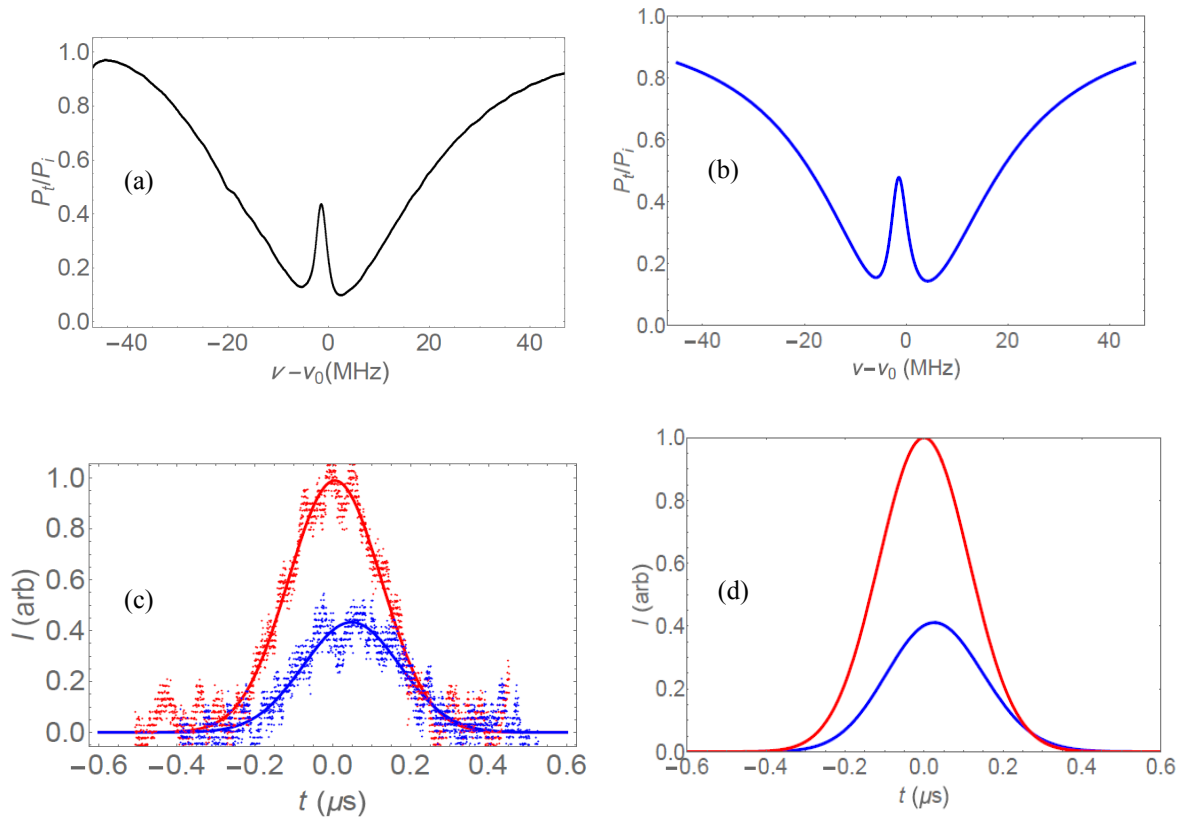


Figure 3. CMIT. (a) Experimental throughput spectrum. (b) Model throughput spectrum. (c) Experimental input and throughput pulses, with a delay of 42 ns. (d) Model input and throughput pulses, with a delay of 40 ns. Parameter values:  $M_1 = 0.87$  (undercoupled),  $M_2 = 0.23$  (undercoupled),  $Q_1 = 4.75 \times 10^6$ ,  $Q_2 = 1.0 \times 10^8$ , offset = -1.5 MHz,  $T_s = 2.2 \times 10^{-8}$ .

In Fig. 3, the fitting is quite reasonable. The width of the transparency window (throughput spike) is somewhat greater than the width of mode 2 in this case. Because  $T_s \gg T_1 T_2 / 4$ , pulse delay is expected.<sup>10</sup> The relatively clean throughput trace indicates little interference with other WGMs, and as a result the predicted delay is nearly the same as the measured delay.

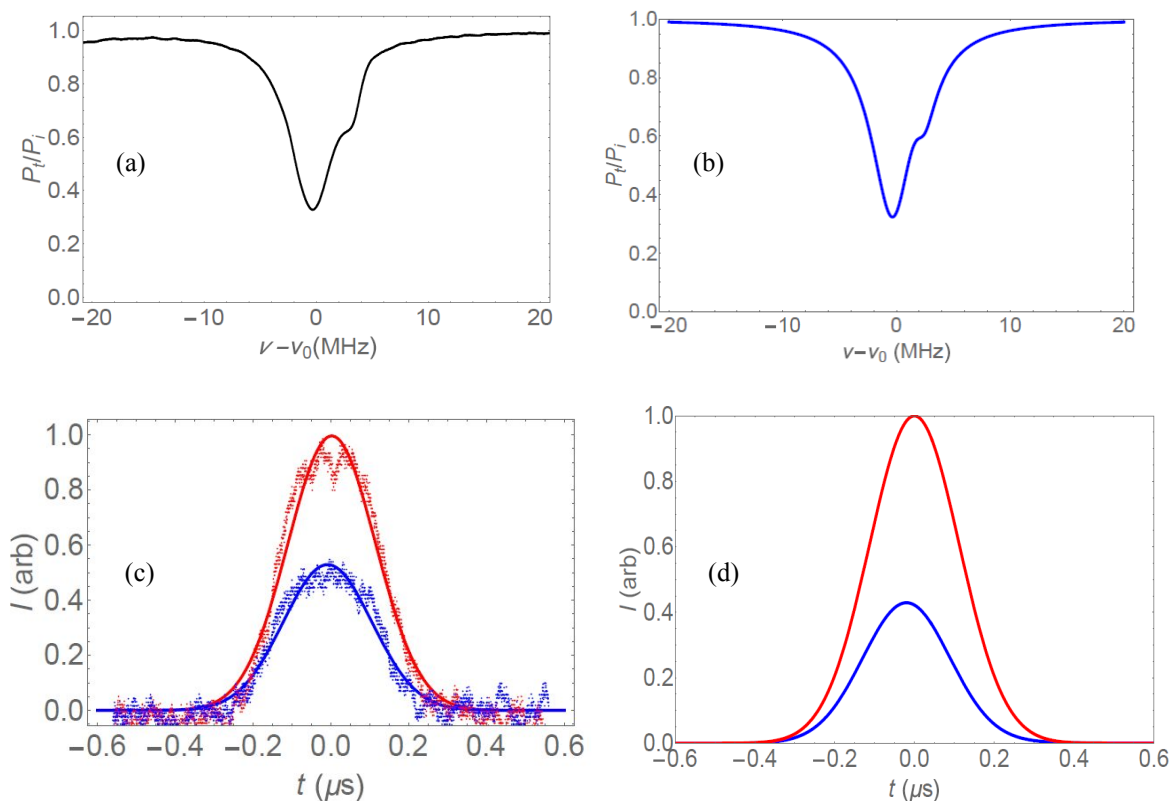


Figure 4. CMIA. (a) Experimental throughput spectrum. (b) Model throughput spectrum. (c) Experimental input and throughput pulses, with an advancement of 11 ns. (d) Model input and throughput pulses, with an advancement of 20 ns. Parameter values:  $M_1 = 0.70$  (undercoupled),  $M_2 = 0.68$  (overcoupled),  $Q_1 = 4.0 \times 10^7$ ,  $Q_2 = 1.0 \times 10^8$ ; offset = 2.0 MHz,  $T_s = 7.9 \times 10^{-10}$ .

In Fig. 4,  $T_2^2/4 < T_s < T_1 T_2/4$ , so pulse advancement is expected, whereas in Fig. 5,  $T_s < T_2^2/4$  and there is delay.<sup>10</sup>

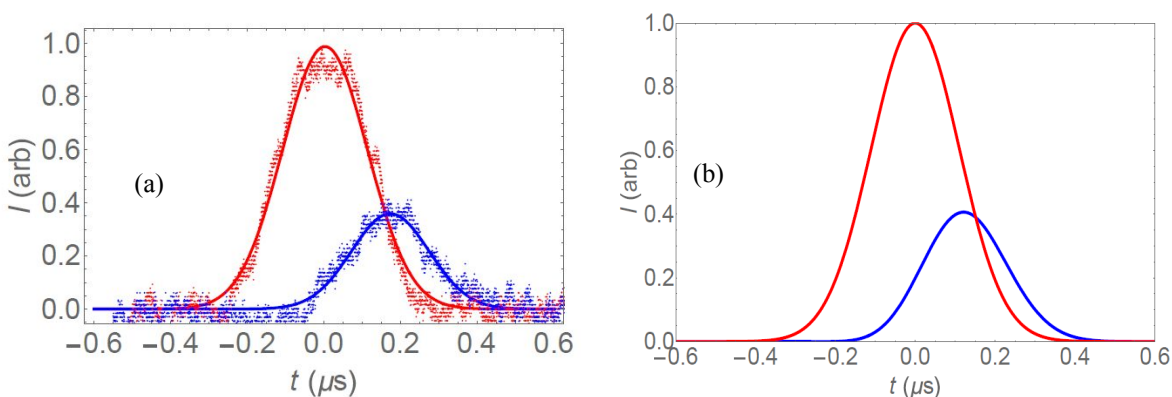


Figure 5. CMIA. (a) Experimental input and throughput pulses, with a delay of 170 ns. (b) Model input and throughput pulses, with a delay of 140 ns. Parameter values:  $M_1 = 0.60$  (overcoupled),  $M_2 = 0.90$  (overcoupled),  $Q_1 = 3.5 \times 10^7$ ,  $Q_2 = 1.0 \times 10^8$ ; offset = -2.0 MHz,  $T_s = 1.0 \times 10^{-10}$ .

## 4.2 CPIT/CPIA

Three examples are presented here. Figure 6 is a case of CPIT, Fig. 7 is CPIA with pulse advancement, and Fig. 8 is CPIA with pulse delay.

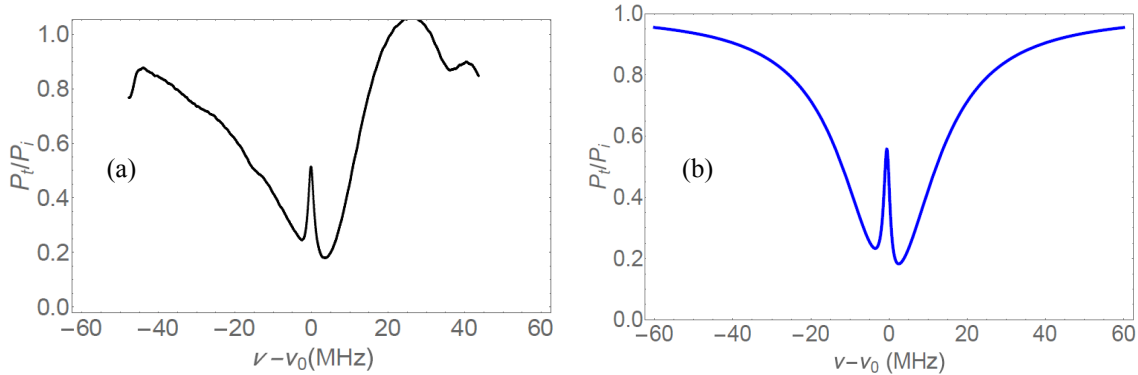


Figure 6. CPIT. (a) Experimental throughput spectrum. (b) Model throughput spectrum. Parameter values:  $M_1 = 0.50$  (overcoupled),  $M_2 = 0.23$  (overcoupled),  $Q_1 = 6.9 \times 10^6$ ,  $Q_2 = 1.0 \times 10^8$ ; offset = -0.5 MHz,  $T_s = 0$ .

The transparency window in Fig. 6 has approximately the same width as mode 2. Since both WGMs in Fig. 6 are overcoupled,  $x_1 x_2 > 1$ , so there is pulse delay.<sup>10</sup> The measured delay is 47 ns, but the model delay is 150 ns. The disagreement is probably a result of the obvious presence of other WGMs, as evident in Fig. 6(a).

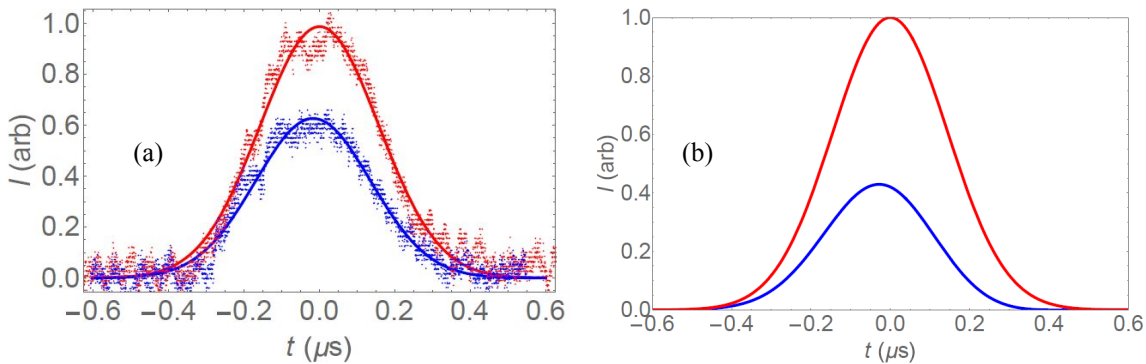


Figure 7. CPIA. (a) Experimental input and throughput pulses, with an advancement of 17 ns. (b) Model input and throughput pulses, with an advancement of 25 ns. Parameter values:  $M_1 = 0.69$  (undercoupled),  $M_2 = 0.64$  (undercoupled),  $Q_1 = 1.8 \times 10^7$ ,  $Q_2 = 1.2 \times 10^8$ ; offset = 1.5 MHz,  $T_s = 0$ .

With both WGMs undercoupled in Fig. 7,  $x_1 x_2 < 1$ , so there is pulse advancement.<sup>10</sup> The minor disagreement probably results from the presence of another WGM in the experimental throughput trace (not shown). In Fig. 8 the value of  $x_1 x_2 > 1$  is not obvious from the coupling regimes, but is shown by calculation, and so there is pulse delay,<sup>10</sup> with good agreement between experiment and model.

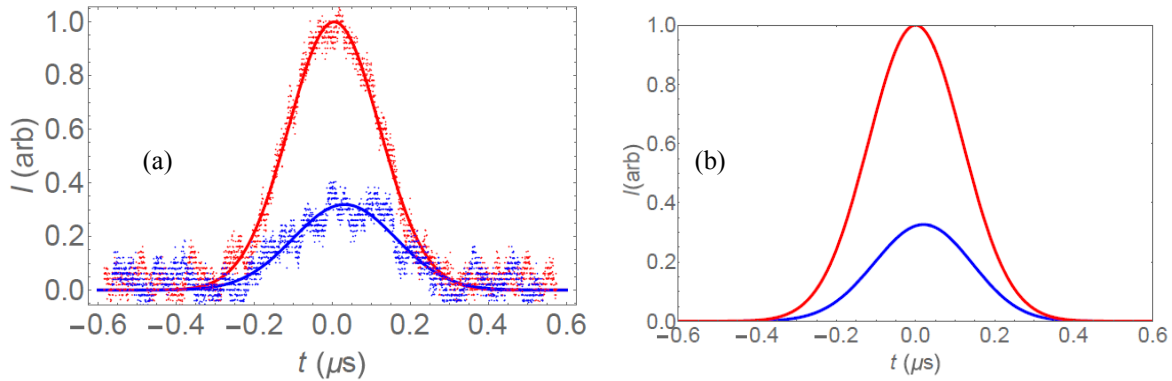


Figure 8. CPIA. (a) Experimental input and throughput pulses, with a delay of 26 ns. (b) Model input and throughput pulses, with a delay of 25 ns. Parameter values:  $M_1 = 0.96$  (undercoupled),  $M_2 = 0.23$  (overcoupled),  $Q_1 = 8.4 \times 10^6$ ,  $Q_2 = 1.0 \times 10^8$ , offset = -1.8 MHz,  $T_s = 0$ .

## 5. DISCUSSION

This work shows how two different methods can produce induced transparency (with pulse delay) or induced absorption (with pulse advancement or delay) by using orthogonally polarized WGMs of a single microresonator. It also demonstrates the utility of the ring cavity model in aiding the understanding of the experimental results. Agreement between model and experiment is seen to be very good when the two WGMs of interest are isolated from other WGMs, and at least reasonable in most other cases.

A comparison of the two methods shows similar throughput spectra and comparable pulse delays and advancements. However, CMIT and CMIA rely on having intermodal coupling as a result of CPC. The strength of (or even existence of) CPC is not predictable for any given pair of coresonant orthogonal WGMs, as it likely depends on details of the spatial overlap (and perhaps phase matching) of the two modes. It's easy to find coresonance, however, so with no (or weak) CPC, CPIT and CPIA can always be found. Since, for example, CPIT also permits tuning of the pulse delay by changing the polarization angle of the input light,<sup>6</sup> it seems that CPIT/CPIA is the more versatile method for achieving and using induced transparency/absorption effects with a single resonator.

It is hoped that these methods for using interacting or superimposed WGMs of a single resonator can contribute to enhanced techniques for sensing. Chemical sensing can be done using frequency-shift or amplitude-change<sup>11</sup> approaches, and fast light (pulse advancement) may be useful for enhancing the response of optical gyroscopes.<sup>12</sup> Of the two methods, CMIA has the tightest constraint on achieving fast light, so the advantage here goes to CPIA.

## ACKNOWLEDGMENT

The authors would like to thank Dr. Razvan-Ionut Stoian for developing the technique for fabricating the HBRs.

## REFERENCES

- [1] Stoian, R.-I., Bui, K. V., and Rosenberger, A. T., "Silica hollow bottle resonators for use as whispering gallery mode based chemical sensors," *J. Opt.* 17, 125011 (2015).
- [2] Fleischhauer, M., Imamoglu, A., and Marangos, J. P., "Electromagnetically induced transparency: Optics in coherent media," *Rev. Mod. Phys.* 77, 633-673 (2005).
- [3] Ilchenko, V. S., Volikov, P. S., Velichansky, V. L., Treussart, F., Lefèvre-Seguin, V., Raimond, J.-M., and Haroche, S., "Strain-tunable high- $Q$  optical microsphere resonator," *Opt. Commun.* 145, 86-90 (1998).

- [4] von Klitzing, W., Long, R., Ilchenko, V. S., Hare, J., and Lefèvre-Seguin, V., “Tunable whispering gallery modes for spectroscopy and CQED experiments,” *New Journal of Physics* 3, 14.1-14.14 (2001).
- [5] Rezac, J. P. and Rosenberger, A. T., “Locking a microsphere whispering-gallery mode to a laser,” *Opt. Express* 8, 605-610 (2001).
- [6] Rosenberger, A. T., “EIT analogs using orthogonally polarized modes of a single whispering-gallery microresonator,” *Proc. SPIE* 8636, 863602-1—863602-11 (2013).
- [7] Rosenberger, A. T., “Effects of polarization mode coupling and superposition in a whispering-gallery microresonator,” *Proc. SPIE* 8998, 899813-1—899813-8 (2014).
- [8] Smith, D. D., Chang, H., Fuller, K. A., Rosenberger, A. T., and Boyd, R. W., “Coupled-resonator-induced transparency,” *Phys. Rev. A* 69, 063804 (2004).
- [9] Naweed, A., Farca, G., Shopova, S. I., and Rosenberger, A. T., “Induced Transparency and Absorption in Coupled Whispering-Gallery Microresonators,” *Phys. Rev. A* 71, 043804 (2005).
- [10] Rosenberger, A. T., “Comparison of methods for achieving induced transparency or absorption with pulse delay or advancement in a single microresonator,” *Proc. SPIE* 9763 (in press).
- [11] Zhou, X., Zhang, L., Armani, A. M., Liu, J., Duan, X., Zhang, D., Zhang, H., and Pang, W., “An Integrated Photonic Gas Sensor Enhanced by Optimized Fano Effects in Coupled Microring Resonators With an Athermal Waveguide,” *J. Lightwave Technol.* 33, 4521-4530 (2015).
- [12] Smith, D. D., Chang, H., Myneni, K., and Rosenberger, A. T., “Fast-light enhancement of an optical cavity by polarization mode coupling,” *Phys. Rev. A* 89, 053804 (2014).